Three-Dimensional Visualization of a Single Block Copolymer in Lamellar Nanodomains

Hiroshi Morita,[†] Toshihiro Kawakatsu,[‡] Masao Doi,[†] Toshio Nishi,[§] and Hiroshi Jinnai*[,||]

Japan Science and Technology Agency and Department of Applied Physics, The University of Tokyo, 7-3-1 Hongo, Bunkyo-ku, Tokyo 113-8656, Japan, Department of Physics, Tohoku Univeristy, Aoba, Aramaki, Aoba-ku, Sendai 980-8578, Japan, Department of Organic and Polymeric Materials, School of Science and Engineering, Tokyo Institute of Technology, 2-12-1, Ohokayama, Meguro-ku, Tokyo 152-8552, Japan, and Department of Macromolecular Science and Engineering, Graduate School of Science and Engineering, Kyoto Institute of Technology, Matsugasaki, Kyoto 606-8585, Japan

Received February 20, 2008; In Final Form May 8, 2008; Revised Manuscript Received May 6, 2008

ABSTRACT: The single-chain distribution in a poly(styrene-*block*-isoprene) block copolymer in the bulk state was studied by the combined method of transmission electron microtomography and three-dimensional mesoscale computer simulations. The local frustration of the block chains on a nanoscale can be analyzed using the size of the gyration radius, R_g. Two representative morphologies in the lamellar morphology have been examined, i. e., flat and bent lamellae. The R_g obtained from the proposed new method gave reasonable agreement with the previously measured values. It was shown that the single polymer chains in the bent lamella is more stretched out than those in the flat lamella. This method provides a new insight into understanding the self-assembled structure in the bulk microdomains.

Introduction

Block copolymers have a tendency to self-assemble, forming films with highly periodic nanoscale morphologies.[1] These films are used as high-functional materials in current nanotechnologies, such as in lithographical templates for the fabrication of quantum dots, in magnetic storage media, in silicon capacitors, etc.[2,3] The functions of these materials are closely related to their morphologies. The subchains of the block copolymers are packed in the microphase-separated domains ("microdomains") with their chemical junctions presumably placed at the interface. Due to such topological constraints, the subchains are sometimes awkwardly accommodated in the nanodomains ("packing frustration").[4] A subtle balance between the interaction (enthalpy) and frustration of the subchains (entropy) determines the final morphologies. Since the packing frustration arises from deviation of the chains from their preferred conformation, scientists have hoped to devise ways to visualize the chain conformation.[5–8]

Small-angle neutron (or X-ray) scattering has been used to evaluate the gyration radius, R_g, of the subchains in a domain structure.[5–8] Hadziioannou et al.[5] and later Hasegawa et al.[7,8] studied the R_g of the subchains in lamellar-forming block copolymers. Their results suggested that the lateral interpenetration of the subchains was smaller than the interpenetration normal to the interface. Although these studies were very carefully carried out, the results seem to be only qualitative due to the imperfect ordering of the lamellae in the block copolymer system. Moreover, the obtained R_g was the averaged value, while R_g is intrinsically a local quantity.

In contrast, a simulation technique has been independently used for investigating the conformation of specific chains in the nanodomains.[9–11] For example, Aoyagi and his co-workers[10] estimated the ratio of the bridge to loop conformations in the lamellar domains of an ABA-type triblock copolymer using the self-consistent field (SCF)[12,13] and the coarse-grained molecular dynamics (CGMD)[9,15] simulations. Their results were in good agreement with the experimental results.[16] The end segment distribution in the lamellar nanodomain of a block copolymer melt was investigated by neutron reflectivity, which also agreed with the results from the SCF simulation.[11] Although the shapes of the interface or the conformations of the subchains are statistically averaged values due to the mean field approximation, these data obtained by the SCF simulation are still the local information. The success of these studies indicates that we are at the stage, where a much closer collaboration between the experiments and SCF simulations is possible.

Recently, extensive progress has been made in the collaboration between the experiments and the SCF simulation. A typical example is the study by Lyakhova et al., who proposed a method to extrapolate the underlying three-dimensional (3D) domain structure from the projection image obtained from the TEM experiments.[17] This idea is very useful because the information, which is not accessible from the experiments, can be consistently estimated under the restriction of the experimental results.

Although transmission electron microtomography (TEMT) provides us with the real 3D nanostructures,[18–20] the single polymer chain in the bulk (inside the microdomains) cannot be directly observed. In the SCF simulation, on the other hand, the chain conformation can be estimated, though the selection of the initial structure, i.e., the nanodomain morphology, may affect the simulation result. Thus, in the present study, we take advantage of the two methods in the sense that the experimentally obtained lamellar nanodomain from TEMT was used as a "boundary condition" for the SCF simulation. Namely, one of the great advantages of our method is that we can analyze the conformation of a subchain localized at a particular point in the real nanodomain, e.g., grain boundary,[21,22] by evaluating its R_g.

Transmission Electron Microtomography (TEMT) Experiments

The sample prepared in this study is the poly(styrene-*block*-isoprene) (SI) block copolymer. The number-averaged molecular weights, M_n, of the PS and PI components are 44 800 and

* To whom correspondence should be addressed. E-mail: hjinnai@kit.ac.jp.
[†] The University of Tokyo.
[‡] Tohoku Univeristy.
[§] Tokyo Institute of Technology.
[||] Kyoto Institute of Technology.

10.1021/ma8003828 CCC: $40.75
Published on Web 06/13/2008

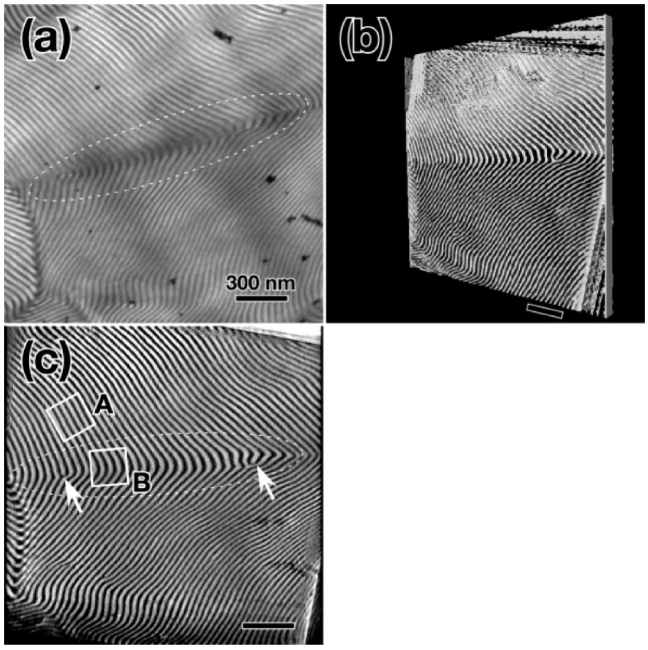

Figure 1. Images obtained by transmission electron microscopy (a) and microtomography (b,c). Scale bars in each figure indicate 300nm. White broken lines in (a) and (c) show the boundary region between two grains, while the squares in (c) indicate the regions to study using the SCF simulations.

43 600, respectively. The molecular weight distribution, M_w/M_n, is 1.02 (M_w is the weight-averaged molecular weight). The SI copolymer shows a lamellar morphology in the bulk state. A film specimen was made by casting the SI block copolymer at 30 °C from a 5% toluene solution. The polymer solution is dried in a vacuum oven at room temperature for a week until a constant weight is attained. The obtained as-cast film is then heated to 140 °C for 24 h in a vacuum. The annealed film of the SI block copolymer is stained with osmium tetraoxide (OsO_4) vapor, embedded in epoxy resin, and ultramicrotomed using a Reichelt−Jung Ultracut-S with a glass knife at ca. −120 °C. The thin sections of ca. 300 nm thickness are placed on copper grids with a polyvinylformal supporting film, coated by carbon, and subjected to observations using a JEOL JEM-1010 transmission electron microscope at an accelerating voltage of 100 kV. Colloidal gold suspensions (10 nm diameter) are placed on the ultrathin sections by drop-casting and allowing the solvent (water) to evaporate (British BioCell GCN005). A series of transmission electron microscopic (TEM) images were acquired at tilt angles ranging from −60° to +60° in 2° increments. The TEM tilt series were aligned by the fiducial marker method and then reconstructed on the basis of the filtered-back-projection method.[20] This process is same as in our previous studies.[20,23,24]

Figure 1a is a TEM micrograph and panels b and c of Figure 1 are the images obtained by the TEMT. In the TEMT images, a grain boundary and a lamellar morphology are clearly observed. Two cubes, A and B, shown in Figure 1c are the regions studied using the 3D SCF simulations. The flat lamella (A) corresponds to the equilibrium lamellar morphology, while the bent lamella (B) corresponds to the grain boundary. Note that the 3D structural data by TEMT is treated as sliced images at even intervals.

SCF Simulation. To perform the SCF simulations, some parameters, such as the Flory−Huggins parameter (χ), number of segments per chain (N), block ratio (f), and the segment length (nm), must be determined. In this study, these parameters can be fixed by the experimental conditions. According to our previous study,[25] the parameters characterizing the polymer

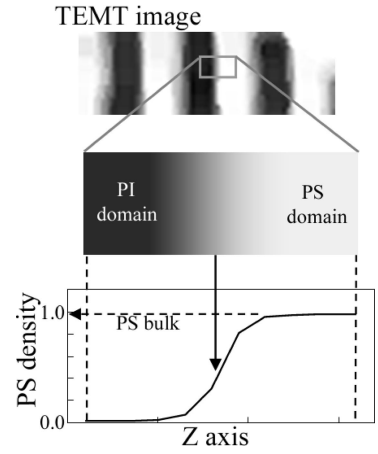

Figure 2. Conversion rule from TEMT image to initial structure for the SCF simulation. This mapping rule is determinded by the comparison between the pixel data of the TEMT image and the density profile of the SCF simulation for the equilibrium structures.

chains used in the TEMT experiments are fixed at $\chi_{PS,PI}N = 44.0$ and $f_{PS} = 0.45$. By use of the SCF simulation with these parameters, the equilibrium lamella structure for the SCF simulation can be obtained by the minimization of the free energy, while the equilibrium lamella structure has already been known by TEMT. The segment length is determined in such a way that the periodic length of the lamella from both the TEMT experiments and the SCF simulations agree.

After the equilibrium structure is obtained by the SCF simulation, the mapping rule can be defined. The density profiles in the TEMT images are represented by pixel data, which must be mapped to the volume fraction of each segment type in the SCF simulation. The mapping rule is determined by comparing the profiles in the equilibrium lamella structure between the TEMT experiments and SCF simulations. The pixel data at the center of the domain in the equilibrium structure obtained by TEMT can map to the density at the central position of the domain in the equilibrium structure by the SCF simulation. The density at the interface is mapped using the rule in which the gradient of the pixel data corresponds to that of the density. The mapping rule formulated by the flat lamella is shown in Figure 2. This rule is applied to the structures A and B shown in Figure 1c. Panels a and d of Figure 3 show the 3D density profile of each block of the flat and the bent lamellar structures obtained from the TEMT experiment. The red and blue regions correspond to the PS and PI nanodomains, respectively.

In general, the experimentally obtained domain structures are not compatible with the periodic boundary condition (PBC) that is usually adopted for the simulation. To avoid the instability associated with an artificial discontinuity at the boundary due to the simple application of PBC, we converted the experimental 3D data to the structural data for the SCF simulation in the following way. Step (1): we set the Z -axis as the direction normal to the layers after rotation of the TEMT images. Step (2): we fixed the size of the simulation box along the Z axis, which is the same as an integer multiple of the lamellar period. In the flat lamellar case, in step (3), the sizes of the simulation box in the X and Y axes have been determined, so that the top and bottom nanodomain structures of the simulation box along these directions are close enough to satisfy the PBC. In the bent lamellar case, we process the images in a slightly different way. For this, in step (3), the position that has the maximum curvature in the X axis is set at the center of the simulation box along the X axis. The obtained structure has almost a plane symmetry against the $Y-Z$ section across the center of the X axis. Step (4): we inserted the extra layer of lattice points at the boundaries

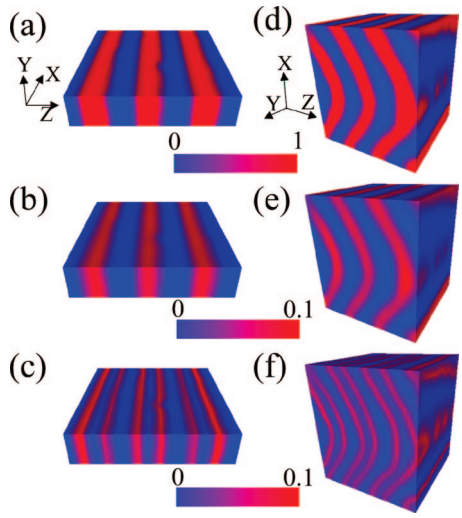

Figure 3. Images obtained by the TEMT and by the self-consistent field simulation: (a−c) and (d−f) are the images of the flat and the bent lamellae A and B, respectively, shown in Figure 1c. The initial structures for the SCF simulation are indicated in (a) and (d), in which the red and blue regions indicate the PS and PI domains. The original sizes of the experimental data for the flat and the bent lamellae are 115.2nm × 28.8nm × 115.2nm and 173nm × 151nm × 151nm, respectively. In the SCF simulation, the simulation box is divided into 64 × 16 × 64 meshes for the flat case (a−c) and 72 × 64 × 64 meshes for the bent case (d−f). (b,e) and (c,f) indicate the results of the end and the junction segment distributions of the PS subchain, respectively.

normal to the X axis in order to adjust the input structure to the PBC. Note that the effect of the artificial extra layer propagated via the mean field potential is negligible in the central region of the simulation box, where the distributions of the chain conformation are evaluated.

In the 3D SCF simulations, the given and optimized fields are the density of the polymer species and the mean field, respectively. This setup is the same as the dynamic SCF technique proposed by Fraaije.[26] We solved the following four coupled equations, eqs 1–4

$$\frac{\partial}{\partial i}Q_K(0,\mathbf{r}_0;i,\mathbf{r}_i)=\left[\frac{b^2}{6}\nabla^2-\beta V_K(\mathbf{r})\right]Q_K(0,\mathbf{r}_0;i,\mathbf{r}_i) \quad (1)$$

$$V_K(\mathbf{r})=\sum_{K'}\chi_{KK'}\varphi_{K'}(\mathbf{r})+\gamma(\mathbf{r}) \quad (2)$$

$$\varphi_K(i,r)=\frac{\int d\mathbf{r}_0\int \mathbf{r}_N Q_K(0,\mathbf{r}_0;i,\mathbf{r}_i)Q_K(i,\mathbf{r}_i;N,\mathbf{r}_N)}{d\mathbf{r}_0\mathbf{r}_N Q_K(0,\mathbf{r}_0;N,\mathbf{r}_N)} \quad (3)$$

$$\varphi_K(\mathbf{r})=\sum_{i\in K}\varphi_K(i,\mathbf{r}) \quad (4)$$

where b is the persistence length, β is $1/k_BT$, $V_K(r)$ is the mean field potential at position $\mathbf{r}$, $Q_K(i, \mathbf{r}_i; j, \mathbf{r}_j)$ is the statistical weight of a K-type subchain between the ith and jth segments at positions $\mathbf{r}_i$ and $\mathbf{r}_j$, respectively, $\chi_{KK'}$ is the Flory−Huggins interaction parameter between K and K' type segments, $\gamma(\mathbf{r})$ is the constraint force due to the incompressibility condition, $\phi_K(r)$ is the total density of the K-type segments, and N is the total number of segments composing the block copolymer chain. Equations 1–4 should be self-consistently solved. In our simulation, $\phi_K(\mathbf{r})$ is provided by the experimental data, and V_K, Q_K, and $\phi_K(i,\mathbf{r})$ are the unknown variables that should be determined by eqs 1–4.[26]

For the density profile, we calculated the most probable distribution of each segment using the SCF simulations. Figure 3b,e shows the distribution of the end segments obtained by such calculations. Note that the end segments are distributed over the entire PS domain. The distribution of the junction segments is displayed in Figure 3c,f. These figures show that the junctions are distributed only in the local interfacial region. These behaviors are consistent with the results of a previous study.[11]

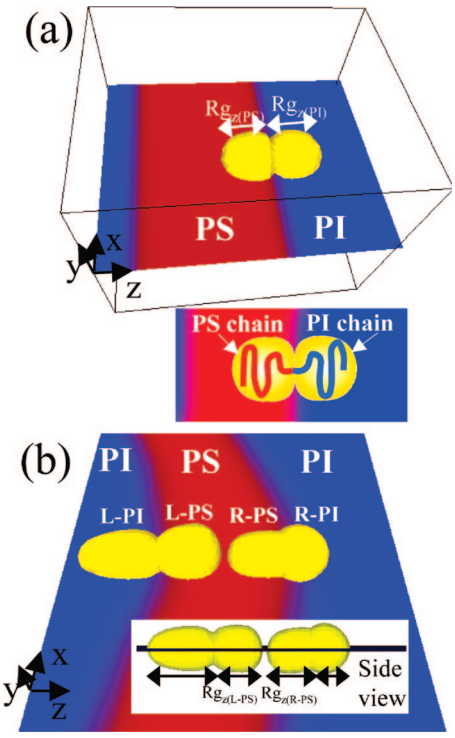

Figure 4. Single chain distribution in (a) the flat and (b) the bent lamellar domains. The density of the PS segments projected on the $X-Z$ plane is shown by the color gradation, and the distribution of single chain $\phi_{single}(\mathbf{r})$ is shown by the yellow contour surfaces where $\phi_{single}(\mathbf{r}) = 0.0003$. Inside the yellow region, 13 and 21% of the total segments of a single chain is included in (a) and (b), respectively. $R_{gz(PS)}$, $R_{gz(L\text{-}PS)}$, and $R_{gz(R\text{-}PS)}$ are estimated to be 2.8, 3.4, and 4.2 nm, respectively.

SCF Simulation for a Single Chain. Using the SCF theory, we can also calculate the segment distribution of a single chain. We considered a single chain, whose junction is located at a certain point ($\mathbf{r} \neq \mathbf{r}_{inter}$) at the interface, and calculated the segment distribution, $\phi_{single}(\mathbf{r})$. This can be justified by the result that the junction segments are localized at the interfaces as shown in Figure 3c,f. We solved a single iteration of eqs 1–4 with the SCF ($V_K(r)$) from a previous simulation under the following constraint conditions:

$$Q(0,\mathbf{r}_0;i_{junction},\mathbf{r})=0 \quad (\mathbf{r}\neq\mathbf{r}_{inter}) \quad (5)$$

$$Q(0,\mathbf{r}_0;i_{junction},\mathbf{r})\neq 0 \quad (\mathbf{r}=\mathbf{r}_{inter}) \quad (6)$$

$$\int \varphi_{single}(\mathbf{r})d\mathbf{r}=1 \quad (7)$$

Figure 4a shows the result of the total segment density distribution of the PS subchain and $\phi_{single}(\mathbf{r})$ under such physical conditions. The total density is shown by the color gradation on the $X-Z$ plane. In order to schematically demonstrate the "shape"of the PS subchain, the isodensity surface corresponding to $\phi_{single}(\mathbf{r}) = 0.0003$ is shown as a yellow surface in the figure. The yellow contour surface is composed of two spheres, each of which corresponds to either the PS or the PI subchain. In the flat lamellar structure, the chains are stretched in the direction normal to the interface layers. Our result of the SCF simulation is consistent with the results in refs and 27. The gyration radius (R_g) was calculated using the $\phi_{single}(\mathbf{r})$. Although meaningful

data for the R_g's for the other two directions (R_{gX}, R_{gY}) cannot be obtained due to the mean field approximation, in which discrete distributions of the polymer chains cannot be represented, R_g for the direction perpendicular to the interface (R_{gZ}) was calculated by the SCF simulation,

$$R_{gZ}^2 = z^2 \varphi_{\text{single}}(\mathbf{r})\mathrm{d}\mathbf{r} \tag{8}$$

where the gyration radius, R_g, in the X direction for a free-standing chain is R_{gX0}.

To check the of the estimated R_g, it was compared to the experimental results of Hasegawa et al.,[7] in which $R_{gZ} = 3.6 \pm 0.2$ nm and $R_{gX0} = 3.0$ nm were obtained using small-angle neutron scattering (SANS) for their SI block copolymer. We have carried out a separate SCF simulation to investigate the results of Hasegawa's experiments using the corresponding parameter sets ($\chi_{PS,\,PI}N = 79.75$ and $f_{PS} = 0.5$). The estimated R_g's are $R_{gZ} = 3.9$ nm and $R_{gX0} = 3.1$ nm. Thus, our simulated values are in excellent agreement with the SANS results.

The same technique was applied to the bent lamellar case (see Figure 4b). We show two chains whose junctions are fixed at the outer (right) and the inner (left) interfaces of the PS nanodomain. The R_{gZ} values of the PS subchains on the left side ($R_{gZ(L\text{-}PS)}$) and right side ($R_{gZ(R\text{-}PS)}$) were 3.4 and 4.2 nm, respectively. The PS subchain of the right side chain (R-PS) is more stretched than that of the left side (L-PS). This is due to the effect of the curvature of the interface. In the bent region, the chains are subjected to a stretching or compressing force arising from the extra gradient of the SCF due to the interfacial curvature, which is caused by the incompressibility condition. This indicates that the local stress in the nanoregion of the deformed structures can be illustrated using the stretching or the compressing conformation of the single chain.

The curvature effect on the periodic length of the lamella was discussed using the experimental data by Knoll et al.[28] In their results, as the curvature of the lamella increased, the periodic length of the lamella also increased. The lamellar period of the PS domain can be roughly estimated as the length of the two PS block chains (four times the gyration radii) in the lamellar structures. Based on our results, the approximated lengths of the PS domain of the flat and bent lamella are 11.2 nm (2.8 nm × 4) and 15.2 nm (3.4 nm × 2 + 4.2 nm × 2), respectively. This indicates that the periodic length of the curved domain is larger than that of the flat domain, which is consistent with those by Knoll et al.[28]

The chain conformation can also be reproduced by the bead-spring model. Letting $\phi_K(i,\mathbf{r})$ be the density of the ith segment of the K-type subchain at position $\mathbf{r}$ obtained from the SCF simulation, we can create an example of the molecular configuration compatible with the given density field using the density-biased Monte Carlo (DBMC) method proposed by Aoyagi et al.[29] Panels a and b of Figure 5 are the snapshots obtained by the DBMC method. In Figure 5a, a typical chain conformation in the flat lamellar domain is also shown for comparison. While the structures shown in Figures 3 and 4 are the statistically averaged ones, the snapshot structure in Figure 5 is the transient one in which a chain conformation may be intuitively understood. Such structures could be used as the initial structure of a future simulation for studying deformation.

Summary

We have proposed a novel method combining the 3D imaging experiments by TEMT and mesoscale simulations to create a picture of the single chains in self-assembled block copolymer nanodomains. The chain conformations inside the nanodomains can be measured at specific points in the morphology. This method has deepened our understanding of the self-assembled structure and also provides hints for improving the material properties. For example, our method will be useful for studying the molecular entanglement of block copolymers at interfaces or at grain boundaries, which are very important regions for the mechanical and transport properties of the materials.

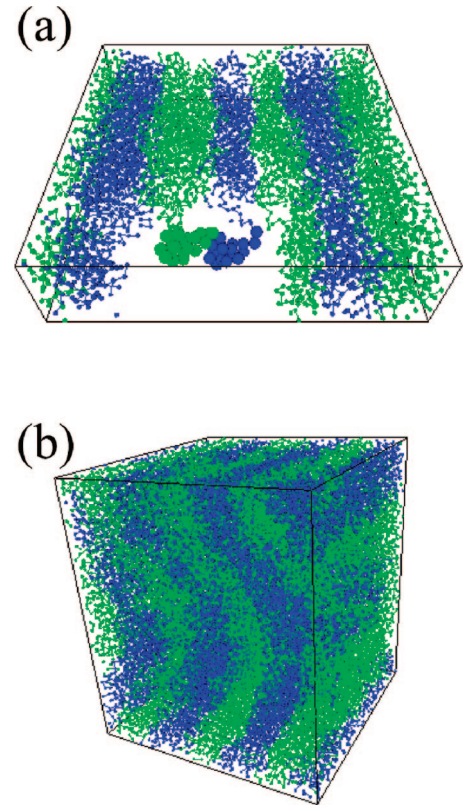

Figure 5. Images obtained by molecular dynamics simulation. In (a) and (b), the polymer chains are represented by the bead-spring model. These structures are obtained using the density biased Monte Carlo method, which is a mapping method based on the common Gaussian nature of the SCF and the bead-spring models.

Acknowledgment. The authors are grateful to NEDO for supporting this study through the Japanese National Project "Nano Structure Polymer Project" by the Ministry of Economy, Trade and Industry. H.J. and T.K. thank the Ministry of Education, Science, Sports and Culture for support through Grants-in-Aid No. 1855019, No. 19031016, and No. 18068002. The authors are grateful to Mr. H. Nishioka, Mr. T. Kaneko, and Mr. K. Niihara for their help with the TEMT experiments. The authors are also grateful to Mr. T. Uneyama for his helpful comments about the simulation.

References and Notes

(1) Thomas, E. L.; Anderson, D. M.; Henkee, C. S.; Hoffman, D. *Nature* **1988**, *334*, 598–601.
(2) Kim, S. O.; Solak, H. H.; Stoykovich, M. P.; Ferrier, N. J.; de Pablo, J. J.; Nealey, P. F. *Nature* **2003**, *424*, 411–414.
(3) Stoykovich, M. P.; Muller, M.; Kim, S. O.; Solak, H. H.; Edwards, E. W.; de Pablo, J. J.; Nealey, P. F. *Science* **2005**, *308*, 1442–1446.
(4) Matsen, M.; Bates, F. S. *Macromolecules* **1996**, *29*, 7641–7644.
(5) Hadziioannou, G.; Picot, C.; Skoukios, A.; Ionescu, M. L.; Mathis, A.; Duplessix, R.; Gallot, Y.; Lingelser, J. P. *Macromolecules* **1982**, *15*, 263–271.
(6) Bates, F. S.; Berney, C. V.; Cohen, R. D.; Wignall, G. D. *Polymer* **1983**, *24*, 519–524.
(7) Hasegawa, H.; Hashimoto, T.; Kawai, H.; Lodge, T. P.; Amis, E. J.; Glinka, C. J.; Han, C. C. *Macromolecules* **1985**, *18*, 67–78.
(8) Hasegawa, H.; Tanaka, H.; Hashimoto, T.; Han, C. C. *Macromolecules* **1987**, *20*, 2120–2127.
(9) Kremer, K.; Grest, G. S. *J. Chem. Phys.* **1990**, *92*, 5057–5086.
(10) Aoyagi, T.; Honda, T.; Doi, M. *J. Chem. Phys.* **2002**, *117*, 8153–8161.
(11) Torikai, N.; Noda, I.; Karim, A.; Satija, A. K.; Han, C. C.; Matsushita,

Y.; Kawakatsu, T. *Macromolecules* **1997**, *30*, 2907–2914.
(12) Helfand, E.; Wasserman, Z. R. *Macromolecules* **1976**, *9*, 879–888.
(13) Hong, K. M.; Noolandi, J. *Macromolecules* **1981**, *14*, 727–736.
(14) Matsen, M. W.; Schick, M. *Phys. Rev. Lett.* **1994**, *72*, 2660–2663.
(15) Grest, G. S.; Kremer, K. *Phys. Rev. A* **1986**, *33*, 3628–3631.
(16) Watanabe, H. *Macromolecules* **1995**, *28*, 5006–5011.
(17) Lyakhova, K. S.; Zvelindovsky, A. V.; Sevink, G. J. A.; Fraaije, J. G. E. M. *J. Chem. Phys.* **2003**, *118*, 8456–8459.
(18) Spontak, R. J.; Williams, M. C.; Agard, D. A. *Polymer* **1988**, *29*, 387–395.
(19) Jinnai, H.; Nishikawa, Y.; Spontak, R. J.; Smith, S. D.; Agard, D. A.; Hashimoto, T. *Phys. Rev. Lett.* **2000**, *84*, 518–521.
(20) Jinnai, H.; Nishikawa, Y.; Ikehara, T.; Nishi, T. *Adv. Polym. Sci.* **2004**, *170*, 115–167.
(21) Jinnai, H.; Sawa, K.; Nishi, T. *Macromolecules* **2006**, *39*, 5815–5819.
(22) Dohi, H.; Kimura, H.; Kotani, M.; Kaneko, T.; Kitaoka, T.; Nishi, T.; Jinnai, H. *Polym. J.* **2007**, *39*, 749–758.
(23) Kawase, N.; Kato, M.; Nishioka, H.; Jinnai, H. *Ultramicroscopy* **2007**, *107*, 8–15.
(24) Niihara, K.; Matsuwaki, U.; Torikai, N.; Atarashi, H.; Tanaka, K.; Jinnai, H. *Macromolecules* **2007**, *40*, 6940–6946.
(25) Morita, H.; Kawakatsu, T.; Doi, M.; Yamaguchi, D.; Takenaka, M.; Hashimoto, T. *Macromolecules* **2002**, *35*, 7473–7480.
(26) Fraaije, J. G. E. M. *J. Chem. Phys.* **1993**, *99*, 9202–9212.
(27) Kawasaki, K.; Kawakatsu, T. *Macromolecules* **1990**, *23*, 4006–4019.
(28) Knoll, A.; Tsarkova, L.; Krausch, G. *Nano Lett.* **2007**, *7*, 843–846.
(29) Aoyagi, T.; Sawa, F.; Shoji, T.; Fukunaga, H.; Takimoto, J.; Doi, M. *Comput. Phys. Commun.* **2002**, *145*, 267–79.

MA8003828